Polymer 68 (2015) 1–10

Contents lists available at ScienceDirect

Polymer

journal homepage: www.elsevier.com/locate/polymer

Curing dependent spatial heterogeneity of mechanical response in epoxy resins revealed by atomic force microscopy

Amir Bahrami [a], Xavier Morelle [b], Lê Duy Hông Minh [a], Thomas Pardoen [b], Christian Bailly [a], Bernard Nysten [a, *]

[a] Institute of Condensed Matter and Nanosciences - Bio-and Soft Matter (IMCN/BSMA), Université catholique de Louvain (UCL), Croix du Sud, 1/L7.04.02 - 1348, Louvain-la-Neuve, Belgium

[b] Institute of Mechanics, Materials and Civil Engineering - Materials and Process Engineering (IMMC/IMAP), Université catholique de Louvain (UCL), place Sainte Barbe, 2/L5.02.02 - 1348, Louvain-la-Neuve, Belgium

ARTICLE INFO

Article history:
Received 21 February 2015
Received in revised form
29 April 2015
Accepted 30 April 2015
Available online 12 May 2015

Keywords:
Epoxy resin
Atomic force microscopy
Crosslinking density

ABSTRACT

The local mechanical properties of partially cured epoxy resins based on tetraglycidyl methylene dianiline (TGMDA) are proved to be heterogeneous at the nanoscale with the degree of heterogeneity decreasing when the crosslinking density increases. The fully cured resin can be considered homogeneous on both the nano- and macroscale. These conclusions are supported by a comprehensive statistical analysis of AFM-based local mechanical properties measurements, which reveal changes in the modulus distributions from multimodal to monomodal. Furthermore, the histograms of adhesion force and energy dissipation exhibit decreasing fluctuations with increasing degree of curing. The surface topography of all samples is very flat at the nanoscale, which indicates that the observed features are not the result of surface irregularities. The existence of differently cured domains due to local fluctuations in the curing kinetics is proposed as the origin of the observed properties contrast.

1. Introduction

Understanding the molecular structure and the properties of epoxies at the micro- and nanoscale in relationship with the mechanical performances has drawn the attention of many researchers since the 1960s [1,2]. Among others, significant efforts have been devoted to address the question whether the molecular structure and properties of epoxies, as a function of scale, are homogeneous or not. In order to generate optimal mechanical and physico-chemical properties, epoxy resins are mostly processed in a highly crosslinked state. Hence, the natural expectation about the molecular structure and resulting properties is a high degree of homogeneity. However, definite confirmation of this expectation is not straightforward and has prompted numerous researches on the subject.

Early structural analyses were performed with the help of electron microscopy on epoxy resins based on diglycidyl ether of bisphenol A (DGEBA) and triglycidyl ether of glycerol (TGEG) crosslinked using various curing programs [3,4]. These studies mostly evidenced a nodular morphology with a length scale between 5 and 60 nm for highly cured resins and related this finding to heterogeneities in the molecular structure due to differences in local crosslinking state. Later, however, other groups raised doubts about these results using structural characterization techniques like small-angle X-ray scattering (SAXS) and small-angle neutron scattering (SANS) [5–7] on DGEBA-based epoxies cured with amine agents. It was claimed that, as a matter of fact, the molecular structure of epoxies and the crosslinking distribution within the cured structure is homogeneous and argued that the previous electron microscopy findings were probably influenced by imaging artifacts due to sample preparation or to the electron interactions with etched surfaces. Nevertheless, there are other proofs of the existence of structural heterogeneities in the literature based on SAXS [8] analysis or comparative studies using both SAXS and SANS [9], which confirmed the presence of a structural heterogeneity on similar epoxy systems. These contradictions highlight the difficulty to reconcile evidences gleaned from different techniques, especially from SAXS and SANS.

* Corresponding author. Tel.: +32 10 473104.
E-mail addresses: amir.bahrami@uclouvain.be (A. Bahrami), xavier.morelle@uclouvain.be (X. Morelle), DuyMinh.Le@soprabanking.com (L.D. Hông Minh), thomas.pardoen@uclouvain.be (T. Pardoen), christian.bailly@uclouvain.be (C. Bailly), bernard.nysten@uclouvain.be (B. Nysten).

http://dx.doi.org/10.1016/j.polymer.2015.04.084
0032-3861/

Addressing the question from a different angle, other researchers hypothesized that if there is any sort of structural heterogeneity in cured epoxies it should be reflected in the physical and mechanical properties. Mijovic et al. [10–12] measured at different temperatures the fracture toughness and dynamic mechanical properties of DGEBA with different curing agents, curing and postcuring programs. They assumed the existence of a heterogeneous nodular morphology with different crosslinking states and established a relationship between the morphology of the fracture surfaces observed by transmission electron microscopy (TEM) and the mechanical properties. In another work, Wu et al. [13] studied the effect of the curing program on the elastic modulus, fracture toughness, impact resistance and glass transition temperature (T_g) of epoxies based on DGEBA crosslinked with two different linear diamines. The morphologies characterized by SAXS were related to the bulk properties.

An epoxy network builds up progressively and passes through partial crosslinking stages with rubbery or glassy dynamics before reaching the maximum crosslinking density [14]. A better understanding of the structure and properties of epoxies must take into account the network formation kinetics. Furthermore, partially cured epoxies have important industrial applications that justify more attention to the link between their molecular structure and their physical as well as mechanical properties, which is the reason why the effect of partial crosslinking on the morphology and properties of epoxies and the progressive network build-up of these resins have been addressed by several authors [15–18].

A survey of previous researches on epoxies shows a lack of comparability among the studies due to the widely different chemical compositions as well as curing and sample preparation schemes. Free surfaces, interfaces formed with different substrates or fracture surfaces were the most widely used sample preparation methods to study various resin systems with a wide variety of crosslinking degree. The experimental plan in each research was adapted to specific needs, which explains also the diversity of approaches and results. Furthermore, most of the previous works were concerned with the relationship between the molecular structure homogeneity and the *macroscopic bulk properties*. Nowadays however, the increasing application of epoxies in many high-tech fields like nanocomposites, or thin adhesive films, asks for considering the *local properties* and their relationship to local scale homogeneity as a central question in this field. A better understanding of the mechanical properties of epoxy resins at the local scale is indeed becoming essential in nanoscience and nanotechnology. Heterogeneities in the local mechanical response can also lead to so-called back stress effects or kinematic hardening which shows up during cyclic loading with a key effect on fatigue resistance properties [19].

Advanced scanning probe microscopy techniques constitute a very attractive approach to unravel local mechanical properties. Early efforts have mostly used tapping-mode atomic force microscopy (TM-AFM) analysis on fractured or etched epoxy surfaces to image the surface topography as well as the phase signal. A nodular morphology was observed on height and phase images taken from the free surface, interface and bulk samples for different epoxy systems [20,21]. The authors suggested the existence of structural heterogeneity at the scale of 75 nm in the case of a bulk sample. Other authors [22], however, studied similar systems and defined a criterion for the presence of a heterogeneous structure based on the difference between the observed features in the height and phase images. Kishi et al. [23] reported an inhomogeneous microstructure in DICY-cured epoxies and related the AFM images to bulk mechanical and physical properties, e.g. fracture toughness, ductility, solvent resistance and heat resistance. Contrast in phase images in AFM tapping-mode is indeed influenced by the local material properties [24–27] and can, in principle, be used as a tool for the detection of heterogeneities in mechanical properties. However, the interpretation of phase images is complicated by the fact that they are also affected by surface physico-chemical properties such as adhesion as well as by the topography. Hence, the observed signal must first be deconvoluted into its various contributions before it can be ascribed to local mechanical heterogeneity.

Recently new AFM modes have been developed for mechanical property mapping, involving the HarmoniX™ mode [28–32], the Peak-Force Quantitative Nanomechanical Mapping (PeakForce-QNM) [33] and the contact resonance [34,35] modes. The aim of these modes is to perform in real-time the decomposition mentioned above by separately measuring different properties like adhesion force, energy dissipation and modulus. Most of these techniques are based on recording and analyzing the force versus distance curves (f–d curves) that result from very shallow indentation of the surface by the AFM tip, as explained later in the experimental section. Haba et al. [36] exploited Peak-Force QNM to study the morphology and mechanical properties of a DGEBA-based epoxy cured with different agents. They used two different tapping forces as well as two different tip sizes in order to verify the possible presence of a nodular morphology and an associated heterogeneity in the mechanical response. Through comparison with typical amorphous polymers, they concluded that epoxies show no heterogeneity in mechanical properties at the local scale and that the observed nodular morphology is essentially an AFM imaging artefact erroneously called “tip convolution”.

The present work aims at clarifying the link between the progressive network build-up of epoxies and the resulting morphology as well as the local mechanical properties homogeneity by using an advanced AFM mode on a well-controlled and representative resin system. The commercial RTM6 epoxy system used as matrix for high performance composites in aerospace applications has been chosen. A range of bulk samples with partial and full curing has been systematically prepared. As flat as possible surfaces were prepared with the help of ultramicrotomy in order to avoid artifacts due to other sample preparation methods, e.g. fracture surfaces, which might be influenced by preferred crack propagation pathways, or chemically etched surfaces, which might alter the true resin structure. High resolution mapping of topography combined with high sensitivity mechanical property mapping were performed using the HarmoniX™ mode. A detailed analysis of topography as well as a cross-correlation of property maps was performed in order to rule out the possible contribution of surface artifacts to the measured properties and to establish a solid relationship between morphology and local mechanical properties.

This analysis shows that the distribution of moduli on stiffness maps changes from bimodal for partially crosslinked samples to monomodal for the fully cured resin. The AFM-extracted modulus for the later sample nicely compares with that obtained from macroscopic tensile tests [37]. These results demonstrate how the homogeneity of the resin local mechanical response changes as a function of crosslinking degree. This is an important result in the context of the current controversies in the literature about epoxy resins opening to several perspectives in the deep understanding of complex mechanical properties such as plasticity initialized by shear transformation, fracture and fatigue influenced by back stress effects.

2. Experimental

2.1. Materials

The experiments have been performed on a premixed epoxy system under commercial name HexFlow® RTM6 supplied by

HEXCEL® Corporation. This high-performance thermoset has been specifically developed for the advanced resin transfer molding (RTM) based processing of carbon fiber reinforced composites used in the aerospace industry. It is composed of a stoichiometric mixture of a tetrafunctional epoxy (tetraglycidyl methylene dianiline, TGMDA) with two amine hardeners (4,4′-methylenebis(2,6-diethylaniline), MDEA, and 4,4′-methylenebis(2-isopropyl-6-methylaniline), M-MIPA), as shown in Fig. 1.

2.2. Curing cycle

The stoichiometric mixture is intended to reach a very high degree of crosslinking, up to 97.5%. In order to study the effect of curing on the morphology and mechanical properties, three different degrees of curing were compared involving two partially cured resins at 70% and 80%; and one resin fully cured at 95%.

Modified curing cycles, compared to the standard program proposed by the supplier, were developed to obtain resins with the desired partial degree of curing. As illustrated schematically in Fig. 2, the reference cycle is composed of three steps: firstly, the resin is degassed for 75 min at 90 °C under vacuum; then, a curing step of 3 h at 130 °C is applied in an air-circulated oven; and, eventually, a post-curing step of 3 h at 180 °C is applied to achieve the maximum crosslinking density. All heating and cooling rates are set to 2 °C/min.

For partial curing, only the degassing and isothermal heating step at 130 °C were applied, but with shorter curing times. The required time to reach a given degree of curing was estimated through the modeling of the crosslinking reaction kinetics, as illustrated in Fig. 2, which was built from the observations and data collected by Skordos et al. [38]. The durations for 70% and 80% curing degrees were respectively, 2 h20 min and 3 h of isothermal heating at 130 °C. The obtained degrees of curing were verified afterwards with differential scanning calorimetry (DSC) (see supplementary information for details).

2.3. Bulk compressive and tensile modulus

The macroscopic compressive and tensile moduli of the fully cured sample were obtained using uniaxial compression test and dynamic mechanical thermal analysis (DMTA), respectively. The compression tests were performed on a screw-driven Zwick-Roell universal testing machine with a 250 kN external load cell, at room temperature with solid lubrication. Tests were carried out at constant crosshead speed of 1 mm/min, on cylindrical specimens with height and diameter both equal to 12 mm. DMTA was performed on a DMA/SDTA861e machine from Mettler Toledo on samples with the following geometry: length 9 mm, width 4 mm, thickness 1 mm. Temperature and frequency sweep analyses were both performed.

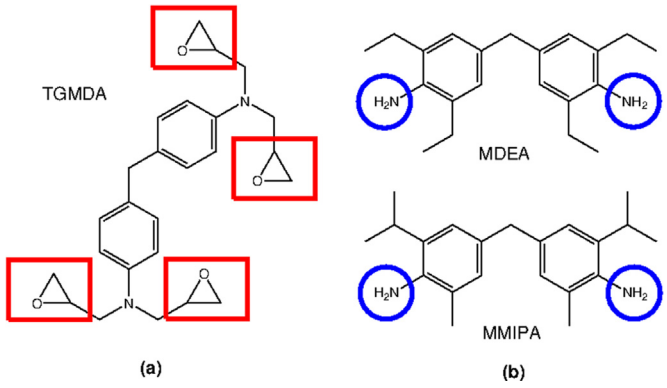

Fig. 1. Chemical structure of (a) the tetrafunctional epoxy resin (tetraglycidyl methylene dianiline, TGMDA) and (b) of its two diamine hardeners MDEA and M-MIPA. The reactive functional groups are marked with rectangles and circles.

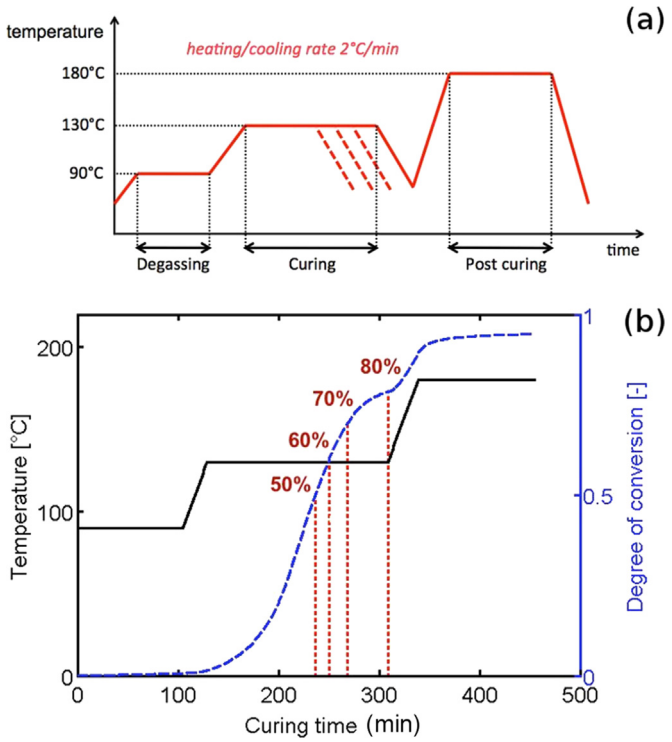

Fig. 2. (a) Typical curing program with three main steps and (b) model of polymerization kinetics for the estimation of the required time to reach a given degree of curing.

2.4. Sample preparation for AFM

Ideal surfaces for mechanical property mapping should be as flat as possible in order to maintain similar tip-sample contact angle and contact area during the scan. Currently, ultramicrotomy is among the best surfacing techniques, as it provides flat surfaces at the nanoscale without considerably altering the structure of the material. Samples were first cut from the cured cylinders, then inserted and fixed to AFM sample holders, and the surface was finally prepared by ultramicrotomy with the help of a diamond knife (LEICA EM FC6 microtome system equipped with DIATOME Cryo 35° knife). The step size in material removal from the surface was set around 50 nm in order to minimize the shear stress on the surface and avoid any material damage. Microtomy was performed at room temperature due to the high glass transition temperature (T_g) of cured epoxy resins (~220 °C). Surfaces were prepared just before the AFM analysis and the microtomed samples were stored in a desiccator to avoid surface contamination.

2.5. AFM characterization

HarmoniX™ mode is a resonant probe AFM technique for higher harmonics imaging of mechanical properties, such as adhesion force, energy dissipation and modulus [29]. In this mode, torsional harmonic cantilevers (THC) are used with the probe tip on one corner of a T-shaped cantilever, which promotes the torsional vibration of the probe during tapping on the sample surface. While tapping near its fundamental flexural resonance frequency

(50 kHz), THC probe indents the sample surface and triggers higher frequency vibrational harmonics of tip-sample interactions. The torsional vibration spectrum of the cantilever is used to reconstruct the force vs. distance ($f-d$) curves. The $f-d$ curves are later analyzed in real time in order to generate maps of different mechanical properties like adhesion force, energy dissipation and DMT modulus (see Supplementary Information for details). HarmoniX™ probes have a wide band width, which offers high force measurement sensitivity in the range of 250 MPa up to 10 GPa. This makes the HarmoniX™ mode a suitable technique for high resolution and fast mapping of mechanical properties on polymers such as epoxy resins.

HarmoniX™ probes with a spring constant of ~2 N/m were used on a Bruker Multimode 5 AFM in order to record images at different magnifications (10×10, 3×3, 1×1 and 0.5×0.5 μm^2) on different areas of the surface of each sample. The image resolution was 256×256 pixels with a scan rate between 0.5 and 1 Hz depending on the image size. The tapping ratio (the ratio of set-point amplitude A_{sp} to free vibration amplitude A_0, $r_{sp} = A_{sp}/A_0$) was set to 0.6 in order to maintain "hard tapping" conditions and to enhance the "material contrast", while keeping a good image resolution.

The photodetector sensitivity was calibrated using a ramping procedure on a clean Si wafer. Afterwards, the cantilever flexural spring constant was calibrated using the thermal tune procedure. The force sensitivity and the dissipation sensitivity were also calibrated through measurement of the jump in the ramping curve on the Si wafer. Finally, the DMT modulus sensitivity was calibrated using a reference polystyrene (PS) sample with known modulus value. The same imaging conditions (tapping ratio and scan rate) were then used for all samples. This careful calibration procedure ensures the extraction of quantitative results.

The tip size of AFM probes used in this study was estimated between 8 and 11 nm using two procedures. First, an absolute tip size measurement was realized by imaging a standard roughness sample from Bruker (RS-12 M). In addition, the tip size was estimated using a relative calibration of the tip size by imaging the standard polystyrene sample.

2.6. Data analysis

A comprehensive analysis was performed on the surface topography, adhesion force, energy dissipation and DMT modulus images in order to address the possible relationships between surface topography and property channels. All analyses were performed based on in-house developed routines under Igor-Pro (WaveMetrics).

2.6.1. Topography images

All images were flattened line-by-line using a 3rd order polynomial fit while masking regions with outliers to avoid introducing artifacts in the analysis. The procedure was applied to 3×3, 1×1 and 0.5×0.5 μm^2 images, because these are the length scales at which the surface topography of the resins is best revealed, while, at the larger length scales, the topography is influenced by

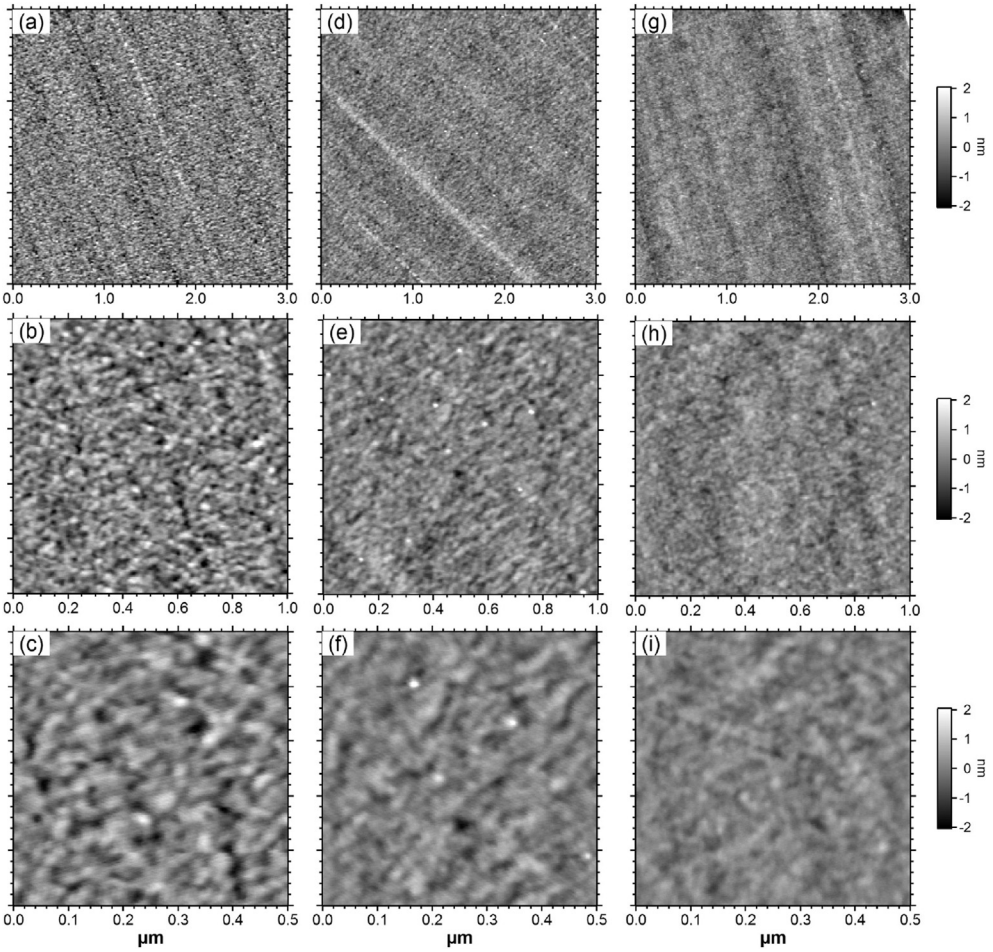

Fig. 3. Topographic images at three magnifications for the three samples with different crosslinking degrees: (a, b, c) 70%, (d, e, f) 80% and (g, h, i) 95%.

scratches due to the microtomy. For all images, the radially averaged power spectral density (PSD) was calculated as

$$PSD(s) = \frac{1}{2\pi}\int_0^{2\pi}\frac{1}{A}\left|\int_A h(\vec{r})\exp(2\pi j\vec{s}\cdot\vec{r})\,\overrightarrow{dr}\right|^2 d\phi \quad (1)$$

where s is the spatial frequency, A is the projected area of the image, and $h(\vec{r})$ is the height function of the image.

Afterwards, the PSDs of individual images (with different length scales) were merged in order to obtain a PSD covering a wider range of spatial frequencies [39]. Considering the surface of the samples as randomly rough surfaces, the PSD curves were fitted using the K-correlation function proposed by Palasantzas et al. [40] to extract the surface characteristic correlation length ξ.

$$PSD(s) = 2\pi\frac{\sigma^2\xi^2}{\left(1+\frac{1}{2H}(2\pi s)^2\xi^2\right)^{1+H}} \quad (2)$$

In this expression H is the roughness exponent related to the slope at high spatial frequencies. The length scale variation of RMS roughness (σ) was also calculated from the merged PSD:

$$\sigma^2(r) = 2\pi\int_{1/r}^{\infty} PSD(s)sds \quad (3)$$

2.6.2. Adhesion force, energy dissipation and DMT modulus images

For each sample an average value of the adhesion, dissipation and DMT modulus was obtained by calculating the average of the mean values obtained for all images. Then, in order to eliminate possible artifacts due to drift, the images were first flattened and then normalized to the average value. One main histogram was then generated by accumulation of the histograms of the image at $1 \times 1\ \mu m^2$. The main histogram was fitted with Gaussian functions. The most probable values and the histogram width were extracted.

3. Results and discussion

3.1. Topography

Fig. 3 shows selected topography images at three different magnifications obtained for the resins cured at 70%, 80% and 95%. The surfaces are flat at the micro- and nanoscale and no extensive scratches or artifacts due to the microtomy are revealed. Apparently, the morphology contrast becomes finer when the degree of curing increases.

The PSD and the RMS roughness variations calculated using the procedure described in the experimental section are shown in Fig. 4. At high spatial frequency (s between ~50 and 100 μm^{-1}) all three samples present the same behavior. In this region that corresponds to small length scales on the images, PSD curves are superimposed and hence the surface roughness of all three samples is similar. The rapid increase of the PSD in this region is followed by a separation of the curves at medium spatial frequencies (s around 30–50 μm^{-1}) and finally by a correlation break (change of slope) where the three samples show differences with a "plateau-like" behavior or a weak frequency dependence. At very low spatial frequencies (s lower than 3 μm^{-1}) there is no meaningful difference between the samples due to highly scattered data points. The larger PSD values for the sample involving low degree of curing correspond to the larger roughness observed at larger length scale. As shown in Fig. 4, the position of the correlation break in the PSD curves, which is related to the correlation length ξ, appears

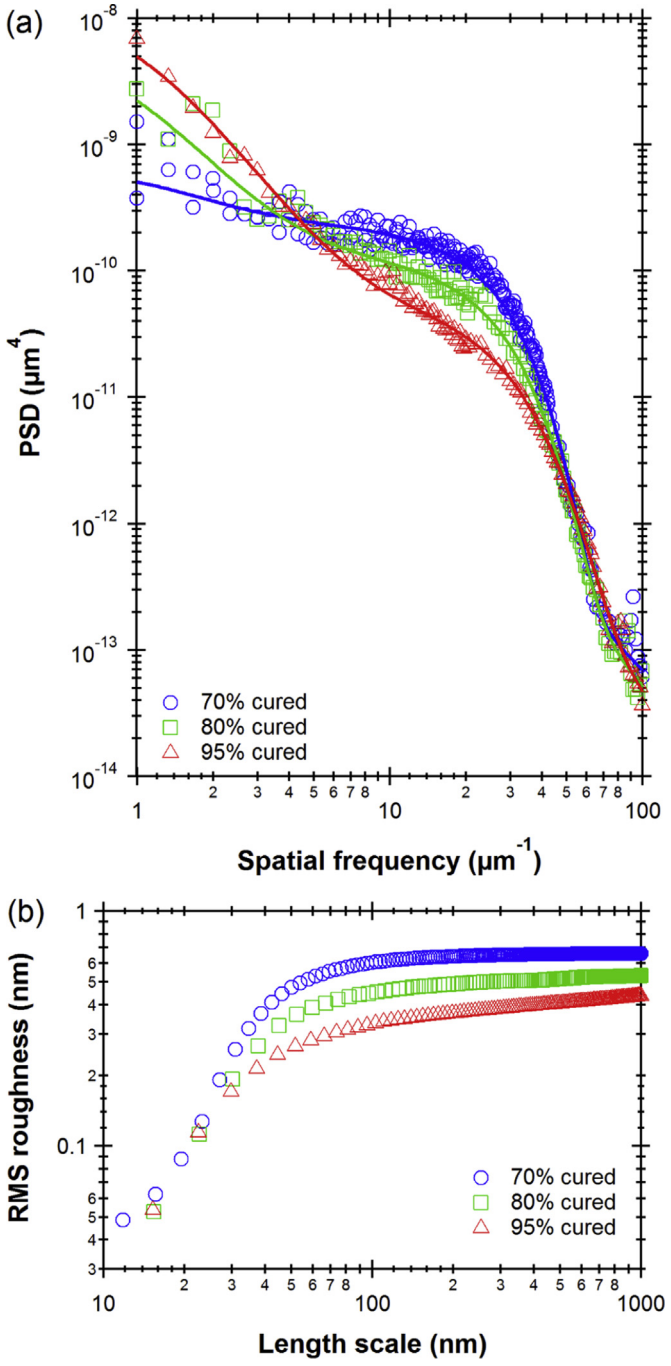

Fig. 4. (a) PSD curves and (b) RMS roughness curves for three samples (blue circles: 70% curing degree, green squares: 80% curing degree, and red triangles: 95% curing degree). On the PSD graph, the solid curves are the results of the fit with the K-correlation function. (For interpretation of the references to color in this figure legend, the reader is referred to the web version of this article.)

Table 1
Results of the fit of the PSD curves with a K-correlation function: RMS roughness (σ) at a scale length of 1 μm, correlation length (ξ) and roughness exponent H.

Curing degree (%)	σ (nm)	ξ (nm)	H
70	0.66	9.6 ± 0.3	6.1 ± 0.6
80	0.53	9.5 ± 0.8	6.0 ± 0.5
95	0.44	8.6 ± 0.9	5.7 ± 0.3

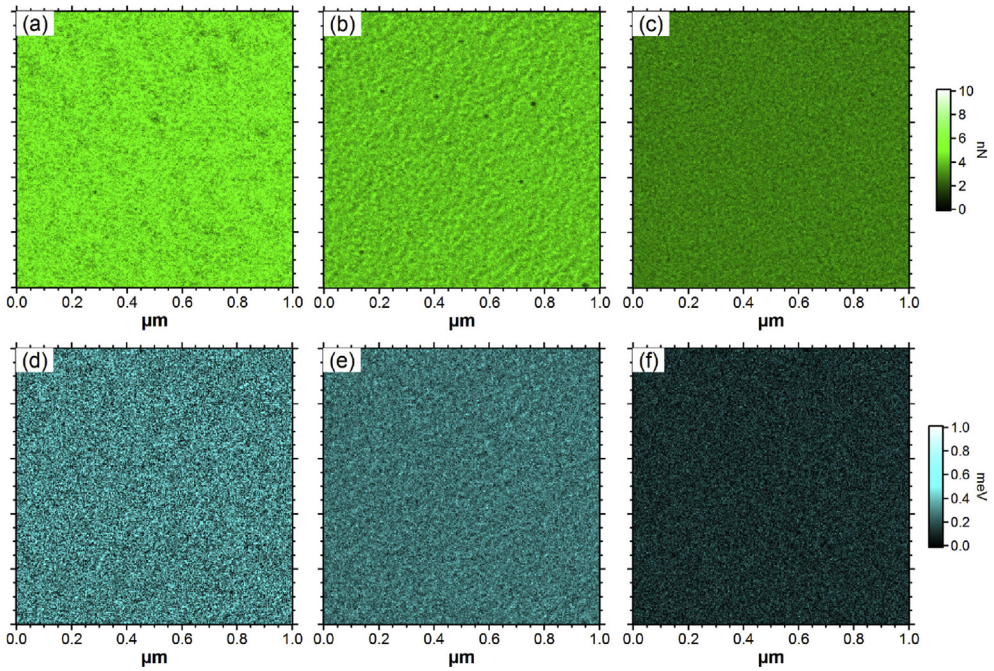

Fig. 5. Adhesion force (top) and energy dissipation (bottom) images for the three samples with different crosslinking degrees: (a, d) 70%, (b, e) 80% and (c, f) 95%.

approximately at the same spatial frequency for all three samples. This is confirmed by the fit of the PSD curves that gives similar values for the correlation length (Table 1).

As indicated, the typical values of σ are relatively low, around ~0.5 nm, which is a proof of the flatness of the surfaces prepared by microtomy. This parameter is a measure of the mean deviation in surface height. The weak difference observed between the samples means that the average height of topography features (nodules or bumps) of the three samples is only marginally different. The correlation length (ξ) is the typical distance between two different irregularities on the surface. Also ξ does not considerably change among the three samples. The subnanometer roughness and the similar lateral size of surface features suggest that if differences appear between the three samples in the property channels (adhesion force, energy dissipation and DMT modulus), this cannot be ascribed to differences in surface roughness of the samples. Especially, the similar roughness of the three samples at the scale of the probe tip, i.e. at large spatial frequency (or small scale length) strongly supports that the property signals are not, or very weakly, influenced by surface topography.

3.2. Adhesion force and energy dissipation

Fig. 5 show the adhesion force and energy dissipation maps at $1 \times 1\ \mu m^2$ scan size for the three samples. A gradual decrease of the values of both parameters with increasing degree of curing can be visually detected through the change in the brightness of the colors. The histograms of the adhesion force and of the energy dissipation, shown in Fig. 6 respectively, exhibit monomodal distributions, with a width and most probable value changing as a function of degree of curing. As described before in the experimental procedures section, a Gaussian function was fitted to these histograms in order to determine the width and maximum of the peak. Table 2 summarizes these values.

The average force of adhesion as well as the average dissipated energy decrease with increasing the curing degree and the deviation on the calculated average values follows the same trend (Fig. 6(c)). As mentioned before, the values of adhesion force and energy dissipation present symmetric distributions around a central value. Nevertheless, the histogram width systematically increases with decreasing the degree of curing. This suggests that there might exist some heterogeneity in the local distribution of these parameters, but not to the extent of breaking the distributions into bimodal or multimodal characteristics.

To understand the origin of the observed variations of the adhesion force and energy dissipation, the type of tip-sample contact should first be clarified in the case of our experiments. In all generality, applying a load to the sample during nanoindentation by AFM may cause three simultaneous and competing processes: (1) elastic energy storage, which is immediately released during unloading; (2) viscoelastic energy storage, which is partly released during unloading (the elastic contribution to viscoelasticity, E') and partly released in long-term (the viscous contribution to viscoelasticity, E''), depending on the unloading rate and on the respective relaxation time of the material; (3) dissipative process or plastic deformation. A key factor that can determine which of the above mentioned processes is mostly influencing the contact, is the indentation rate. A study by Tranchida et al. [41] on various polymers covering a wide range of mechanical response shows that during indentation with rates above 10 Hz, which is much lower than the HarmoniX™ indentation rate of ~50 kHz, the contribution of viscoelastic and plastic phenomena can be reasonably neglected and the contact can thus be considered as dominated by elastic processes.

Thus, the energy dissipation ascribed to either viscoelasticity/plasticity or adhesion force or to a mixture of both (see Supplementary Information) is mostly due to the adhesion force in the case of our experiments. This may explain the fact that both properties present the same trends as a function of the crosslinking degree. Furthermore, this suggests that the measured adhesion force is mostly due to chemical interactions rather than to viscoelastic phenomena. The elastic dominated contact, in addition, proves that the tip-sample contact can indeed be analyzed here with elastic contact models such as the DMT model (see Supplementary Information).

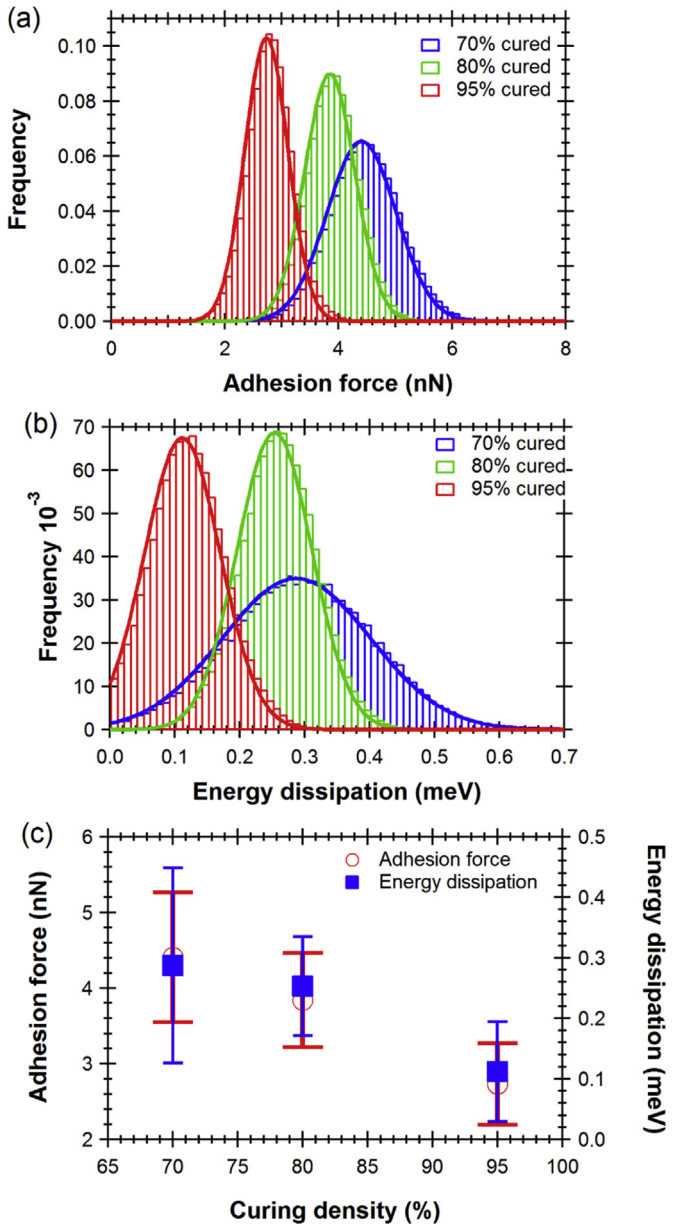

Fig. 6. Histograms of (a) the adhesion force and (b) the energy dissipation for the three samples. (c) Variation of the peak values of the adhesion force and the energy dissipation with the crosslinking degree; the error bars corresponds to the Gaussian width of the histograms.

3.3. DMT modulus

Fig. 7 shows the DMT modulus maps of all samples in three scan sizes. An apparent gradual increase of the modulus with increasing degree of curing is observed as shown by the change in the color brightness of the images. The images at smaller scales (1×1 and 0.5×0.5 μm^2) also suggest the presence of stiffer and more compliant domains, especially for the samples with 70% and 80% crosslinking density. The apparent size of these domains is around 20–30 nm.

The histograms of DMT modulus reveal different behaviors between the samples, changing from clearly bimodal to monomodal as the crosslinking degree increases (Fig. 8). Unlike the adhesion force and energy dissipation, the DMT modulus presents a bimodal distribution for the 70% and 80% curing with two clearly distinct peaks while it is monomodal with a single peak for the 95% curing degree.

Globally, the average value of the DMT modulus increases with the degree of curing. The corresponding distributions have been fitted with a series of Gaussian functions. Fig. 8(a and b) show the Gaussian fit of the modulus histograms for the 70% and 80% crosslinked samples. These two samples exhibit bimodal distributions with peaks located around 2400 MPa and 3100 MPa, confirming the presence of stiffer and more compliant domains. The proportion of stiff domains increases from 0.52 for the sample with 70% curing degree to 0.74 for the sample with 80% curing degree. A similar analysis for the 95% sample (Fig. 8(c)) with only one Gaussian function gives a most probable value around 3200 MPa, corresponding only to stiff domains. The most probable values and the peak proportion for all samples are summarized in Table 3.

This evolution is illustrated in Fig. 9 where the most probable values of the peaks are reported as a function of the curing degree. On this graph, the size of the symbols is proportional to the fraction of the corresponding peak and the error bars to the width of the peaks. One can see that there are two main populations of modulus values around 2400 MPa and 3100 MPa. The fraction of stiffer domains increases upon increasing the degree of curing; likewise, the fraction of more compliant domains gradually decrease from 70% to 80% curing degree and finally disappears for the 95% cured sample.

Based on the assumptions that the stiffer and more compliant domains are characterized by an essentially constant local degree of crosslinking and that it is the fractions of the two types of domains that changes with the global degree of crosslinking, the crosslinking degree of the compliant domain can be estimated using a simple linear regression. Using the ratio of the compliant domains for the three global degrees of crosslinking (Table 3), we can extrapolate the hypothetical global degree of curing for the case where the sample would consist only of one compliant domain, which would correspond to an estimated degree of crosslinking of about 46% (see Supplementary Information). Hence, it can be argued that the local structure of incompletely cured RTM6 resins probably consists of contiguous domains with a size of the order of 20–30 nm involving very high and comparably low degree of crosslinking.

However, the determination of the bulk modulus of a sample cured only at 46% was impossible due to the very brittle nature of lightly crosslinked samples that strongly limits standard test specimen preparation. However, based on the available literature data and the presented results of this work, we may have a rough estimation of the modulus for a bulk sample with 46% curing degree. As discussed by Mooseburger et al. [16], the gel point in RTM6 epoxy systems is reached typically between 40% and 50% of conversion. Thus, 46% of crosslinking should be above the gel point. The measurements performed by this group showed that the macroscopic moduli change by 23% as the curing degree increases from 55% to 95%. The two values reported here for the moduli corresponding to the fully cured and lightly cured domains fall in this reported range.

The origin of the observed heterogeneity most probably is related to the peculiar reaction kinetics of epoxy-amine systems. It

Table 2
Summary of the calculated values obtained by fitting the adhesion force and energy dissipation histograms with Gaussian functions: average adhesion force F_{adh}, average energy dissipation E_{diss}, $\triangle F_{adh}$ and $\triangle E_{diss}$ width of the Gaussian functions.

Curing degree (%)	F_{adh} (nN)	$\triangle F_{adh}$ (nN)	E_{diss} (meV)	$\triangle E_{diss}$ (meV)
70	4.40	0.86	0.29	0.16
80	3.84	0.63	0.25	0.08
95	2.73	0.54	0.11	0.08

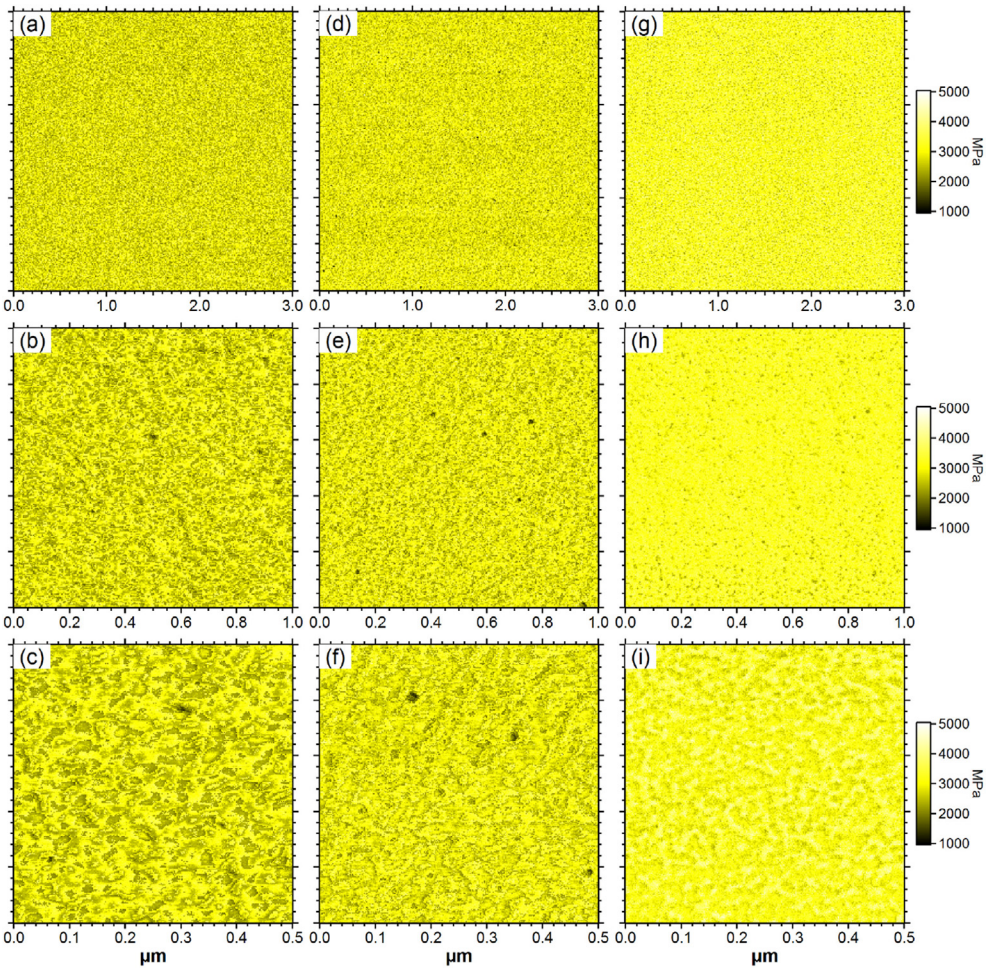

Fig. 7. DMT modulus images at three magnifications for the three samples with different crosslinking degrees: (a, b, c) 70%, (d, e, f) 80% and (g, h, i) 95%.

has been shown that the curing reaction of RTM6 is partially auto-catalyzed [42]. In other words, the already reacted groups accelerate the reaction. However, the low molecular mobility in the reaction medium from the gel point and above prevents effective diffusion of the auto-catalyzing agents, which can cause spatial modulation of the reactivity in the system. This, in turn, generates spatial heterogeneity of the degree of crosslinking. Nevertheless, as shown in this work, this heterogeneity decreases with increasing the global curing degree as deduced from the narrower adhesion force and energy dissipation histograms as well as from the monomodal DMT modulus distribution for the fully crosslinked sample. The AFM extracted modulus value for the 95% cured sample compares very well with that measured by macroscopic tensile testing. This strongly suggests that the fully cured sample is mechanically homogeneous from the scale of nanoindentation by the AFM tip up to the macroscopic scale of tensile test specimens, i.e. from a few nanometers up to several millimeters [43].

A comparison of the bulk compressive and tensile moduli of the 95% cured sample with the AFM-extracted values has also been done. A systematic comparison of bulk and AFM-extracted moduli for all three samples has not been performed. Indeed, first a local-global comparison for partially cured samples (70% and 80%) is not straightforward due to the heterogeneous nature of these two samples. Furthermore, in the case of those samples, machining of standard specimens was not possible due to their brittleness.

The AFM-measured modulus is compared to the bulk compressive and tensile moduli in Table 4. The measured bulk compressive and tensile moduli of the 95% cured sample, 3070 MPa and 2700 MPa respectively, are close to the literature value of 2890 MPa [44,45]. The difference between the compressive and tensile moduli is originating from different testing set-up and loading of the specimens. The AFM-extracted local modulus is higher than the bulk compressive and tensile moduli by 5.2% and 19.6% respectively. Nevertheless, the local and bulk values are comparable and the observed differences could be attributed to the differences between the methods of measurements. The similarity in local and bulk moduli is another proof of homogeneity of the mechanical response over different length scales. As mentioned in the main text, the fully cured sample does not show any sign of heterogeneity in the local mechanical response at the scale of AFM tip size.

4. Conclusions

The HarmoniX™ mode of atomic force microscopy has been used to study the effect of the degree of crosslinking on the local morphology and mechanical properties of RTM6 epoxy resin. A comprehensive analysis of the surface topography, aiming at ruling out the possible influence of the surface topography on the measured properties, together with a statistical analysis of the properties was carried out.

Microtomy allowed obtaining very smooth surfaces with sub-nanometer roughness. A very slight increase of the sample surface roughness was observed with the decrease of the curing degree, with the RMS roughness ranging from ~0.4 nm for the fully cured

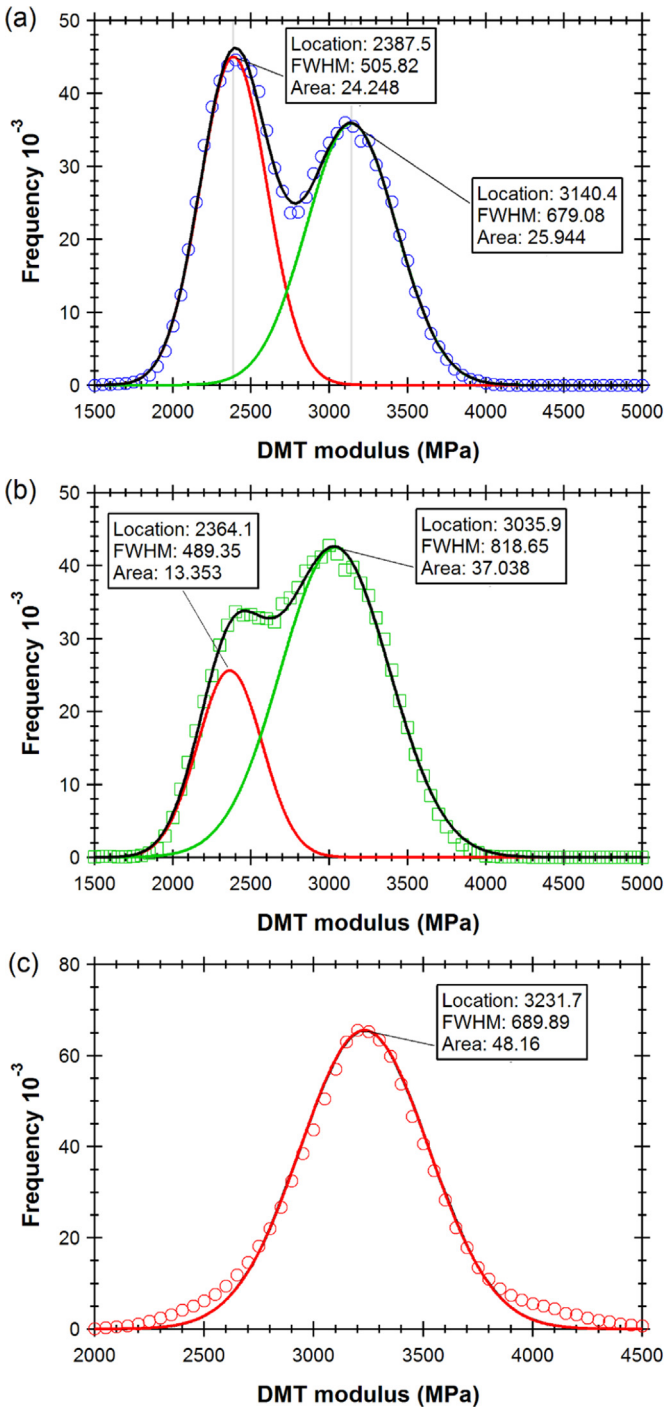

Fig. 8. DMT modulus histograms for crosslinking degrees: (a) 70%, (b) 80% and (c) 95%. The symbols correspond to the experimental data and the solid lines are the results of the fits with series of Gaussian functions (two for 70% and 80% degree of curing and one for 95% degree of curing).

Table 3
Summary of the calculated values obtained by fitting the DMT modulus histograms with Gaussian functions: peak 1 position, E_1, and fraction and peak 2 position E_2 and fraction.

Curing degree (%)	E_1 (MPa)	Peak 1 fraction (%)	E_2 (MPa)	Peak 2 fraction (%)
70	2390	48	3140	52
80	2360	26	3040	74
95	–	–	3230	100

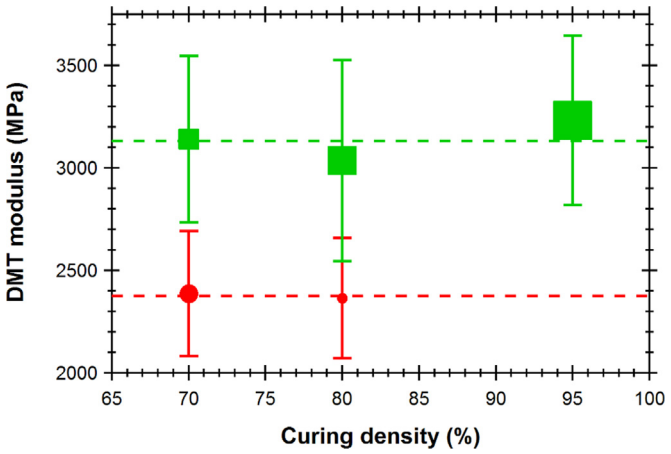

Fig. 9. Variation with the crosslinking density of the peak values of the two populations at around 2400 MPa and 3100 MPa. The contribution of each population is highlighted via the size of symbols and the error bars correspond to the with of the corresponding Gaussian function.

sample to ~0.6 nm for 70% curing degree. The lateral size of the surface features contributing to the roughness was found to be similar for all samples with an average size (correlation length) around ~9 nm. It can be thus expected that the mechanical properties signals (adhesion, energy dissipation and DMT modulus) are not influenced by the surface topography.

The images of the adhesion force and the energy dissipation exhibit homogeneous morphologies for all curing programs, as evidenced by monomodal distributions of the corresponding histograms. The average values of adhesion force and energy dissipation as well as the corresponding deviations decrease as the curing degree increases. The high frequency property mapping of the HarmoniX™ mode, around 50 kHz, ensures an elastic dominated tip-sample contact with negligible viscoelastic and plastic contributions. Chemical interactions are thus the main origin of the detected adhesion force and the decrease of the energy dissipation is directly due to the decrease of the adhesion force.

On the contrary, the analysis of the DMT modulus images reveals a clearly bimodal distribution for the non-fully cured resins (70% and 80%) while the distribution is monomodal for the fully cured sample (95%). The analysis of the histograms gives values around 2400 MPa and 3100 MPa for the two peaks observed on the non-fully cured samples. These values are attributed to the co-existence of “more compliant” non-fully cured domains and of “stiffer”, almost fully cured, domains. The fraction of the “more compliant” domains decreases with increasing the degree of curing and, finally, these domains disappear at full curing. A rough estimation of the degree of curing of the compliant domains is about 46%. A possible explanation for the observed heterogeneity can be found in the kinetics of curing of epoxy resins. The localized auto-catalysis by the already reacted groups in a low molecular mobility reaction medium promotes local heterogeneities in the curing evolution and hence in the resulting mechanical response. This phenomenon can form distinct compliant and rigid “domains” with low and high crosslinking degrees.

These results show how the difference in the degree of curing of epoxy resins can influence the local heterogeneities in the

Table 4
Comparison between the AFM-measured modulus with the bulk compressive and tensile moduli of the 95% cured resin.

AFM-extrated modulus (MPa)	Bulk compressive modulus (MPa)	Bulk tensile modulus (MPa)
3230	3070	2700

mechanical response. The fully cured resins can indeed be considered as homogeneous at the nanoscale. In addition, it was shown that AFM-based approaches to the local property mapping of epoxies are powerful tools for addressing such a complicated issue involving heterogeneities at the nanoscale.

Acknowledgments

Kind helps of Pascale Lipnik for microtomy preparations as well as valuable helps of Benoit Wucher for the modeling of the curing kinetics of RTM6 were greatly appreciated.

The partial support of the Fonds de la Recherche Scientifique – F.R.S. – FNRS – through FNRS scholarship and of the Belgian Federal Science Policy (IAP-PAI 7/05) are gratefully acknowledged.

Appendix A. Supplementary data

Supplementary data related to this article can be found at http://dx.doi.org/10.1016/j.polymer.2015.04.084.

References

[1] Cuthrell RE. Epoxy polymers. ii. Macrostructure. J Appl Polym Sci 1968;12:1263–78. http://dx.doi.org/10.1002/app.1968.070120601.
[2] Kenyon AS, Nielsen LE. Characterization of network structure of epoxy resins by dynamic mechanical and liquid swelling tests. J Polym Sci Part A Polym Chem 1969;3:275–95. http://dx.doi.org/10.1080/10601326908053811.
[3] Racich JL, Koutsky JA. Nodular structure in epoxy resins. J Appl Polym Sci 1976;20:2111–29. http://dx.doi.org/10.1002/app.1976.070200808.
[4] Aspbury PJ, Wake WC. The supermolecular structures found in cured epoxy resins. Polym Int 1979;11:17–27. http://dx.doi.org/10.1002/pi.4980110105.
[5] Dušek K, Pleštil J, Lednický F, Luňák S. Are cured epoxy resins inhomogeneous? Polymer 1978;19:393–7. http://dx.doi.org/10.1016/0032-3861(78)90243-4.
[6] Dušek K. Are cured thermoset resins inhomogeneous? Angew Makromol Chem 1996;240:1–15. http://dx.doi.org/10.1002/apmc.1996.052400101.
[7] Bai SJ. Crosslink distribution of epoxy networks studied by small-angle neutron scattering. Polymer 1985;26:1053–7. http://dx.doi.org/10.1016/0032-3861(85)90228-9.
[8] Matyi RJ, Uhlmann DR, Koutsky JA. Structure of glassy polymers. vii. small-angle x-ray scattering from epoxy resins. J Polym Sci Part B Polym Phys 1980;18:1053–63. http://dx.doi.org/10.1002/pol.1980.180180512.
[9] Wu W-L, Bauer BJ. Network structure of epoxies – a neutron scattering study: 2. Polymer 1986;27:169–80. http://dx.doi.org/10.1016/0032-3861(86)90322-8.
[10] Mijovic J, Koutsky JA. The effect of postcure time on the fracture properties and nodular morphology of an epoxy resin. J Appl Polym Sci 1979;23:1037–2014. http://dx.doi.org/10.1002/app.1979.070230408.
[11] Mijovic J, Koutsky JA. Correlation between nodular morphology and fracture properties of cured epoxy resins. Polymer 1979;20:1095–107. http://dx.doi.org/10.1016/0032-3861(79)90301-X.
[12] Mijovic J, Tsay L. Correlations between dynamic mechanical properties and nodular morphology of cured epoxy resins. Polymer 1981;22:902–6. http://dx.doi.org/10.1016/0032-3861(81)90265-2.
[13] Wu W-L, Hu J-T, Hunston DL. Structural heterogeneity in epoxies. Polym Eng Sci 1990;30:835–40. http://dx.doi.org/10.1002/pen.760301406.
[14] Yoon SS, Yu WJ, Kim HC. Phase transition of epoxy resin during isothermal curing monitored and by ultrasonic velocity measurements. J Mater Sci Lett 1992;11:1392–4. http://dx.doi.org/10.1007/BF00729372.
[15] Vanlandingham MR, Eduljee RF, Gillepsie JWJ. Relationships between stoichiometry, microstructure, and properties for amine-cured epoxies. J Appl Polym Sci 1999;71:699–712. http://dx.doi.org/10.1002/(SICI)1097-4628(19990131)71.5\%3C699::AID-APP4\%3E3.0.CO;2-D/full.
[16] Moosburger-Will J, Greisel M, Sause MGR, Horny R, Horn S. Influence of partial cross-linking degree on basic physical properties of RTm6 epoxy resin. J Appl Polym Sci 2013;130:4338–46. http://dx.doi.org/10.1002/app.39722.
[17] Moosburger-Will J, Greisel M, Horn S. Physical aging of partially crosslinked RTm6 epoxy resin. J Appl Polym Sci 2014;131:41121. http://dx.doi.org/10.1002/app.41121.
[18] Sahagun CM, Knauer KM, Morgan SE. Molecular network development and evolution of nanoscale morphology in an epoxy-amine thermoset polymer. J Appl Polym Sci 2012;126:1394–405. http://dx.doi.org/10.1002/app.36763.
[19] Morelle XP, Bahrami A, Lani F, Melchior MA, Nysten B, Bailly C, et al. Characterization and modeling of the time-dependent behavior of the rtm6 structural epoxy involving recovery and back stress. In: ECCM16-16th European conference on composite materials, Seville (Spain); June 22-26, 2014.
[20] Gu X, Ho D, Sung L, VanLandingham MR, Nguyen T, Raghavan D. Nanocharacterization of surface and interface of different epoxy networks. In: Karim A, Frank C, Russell T, P.F N, editors. MRS symposium DD polymer interfaces and thin films, vol. 710. Materials Research Society; 2002. p. 153–8.
[21] Gu X, Nguyen T, Oudina M, Martin D, Kidah B, Jasmin J, et al. Microstructure and morphology of amine-cured epoxy coatings before and after outdoor exposures – an afm study. J Coat Technol Res 2005;2:547–56. http://dx.doi.org/10.1007/s11998-005-0014-x.
[22] Duchet J, Pascault JP. Do epoxy-amine networks become inhomogeneous at the nanometric scale? J Polym Sci Part B Polym Phys 2003;41:2422–32. http://dx.doi.org/10.1002/polb.10585.
[23] Kishi H, Naitou T, Matsuda S, Murakami A, Muraji Y, Nakagawa Y. Mechanical properties and inhomogeneous nanostructures of dicyandiamide-cured epoxy resins. J Polym Sci Part B Polym Phys 2007;45:1425–34. http://dx.doi.org/10.1002/polb.21170.
[24] Magonov S, Elings V, Whangbo M-H. Phase imaging and stiffness in tapping-mode atomic force microscopy. Surf Sci 1997;375:L385–91. http://dx.doi.org/10.1016/S0039-6028(96)01591-9.
[25] Scott WW, Bhushan B. Use of phase imaging in atomic force microscopy for measurement of viscoelastic contrast in polymer nanocomposites and molecularly thick lubricant films. Ultramicroscopy 2003;97:151–69. http://dx.doi.org/10.1016/s0304-3991(03)00040-8.
[26] Zhao Y, Cheng Q, Qian M, Cantrell JH. Phase image contrast mechanism in intermittent contact atomic force microscopy. J Appl Phys 2010;108:094311. http://dx.doi.org/10.1063/1.3503478.
[27] Raghavan D, Gu X, Nguyen T, VanLandingham M, Karim A. Mapping polymer heterogeneity using atomic force microscopy phase imaging and nanoscale indentation. Macromolecules 2000;33:2573–83. http://dx.doi.org/10.1021/ma991206r.
[28] Sahin O, Atalar A. Simulation of higher harmonics generation in tapping-mode atomic force microscopy. Appl Phys Lett 2001;79:4455–7. http://dx.doi.org/10.1063/1.1429296.
[29] Sahin O, Magonov S, Su C, Quate CF, Solgaard O. An atomic force microscope tip designed to measure time-varying nanomechanical forces. Nat Nanotechnol 2007;2:507–14. http://dx.doi.org/10.1038/nnano.2007.226.
[30] Sahin O. Harnessing bifurcations in tapping-mode atomic force microscopy to calibrate time-varying tip-sample force measurements. Rev Sci Instrum 2007;78:103707. http://dx.doi.org/10.1063/1.2801009.
[31] Sahin O, Erina N. High-resolution and large dynamic range nanomechanical mapping in tapping-mode atomic force microscopy. Nanotechnology 2008;19:445717. http://dx.doi.org/10.1088/0957-4484/19/44/445717.
[32] Sahin O. Time-varying tip-sample force measurements and steady-state dynamics in tapping-mode atomic force microscopy. Phys Rev B 2008;77:115405. http://dx.doi.org/10.1103/PhysRevB.77.115405.
[33] Minne S, Hu S, Pittenger B, Su C. Nanoscale quantitative mechanical property mapping using peak force tapping atomic force microscopy. Microsc Microanal 2010;16:464–5. http://dx.doi.org/10.1017/S1431927610061829.
[34] Killgore JP, Yablon DG, Tsou AH, Gannepalli A, Yuya PA, Turner JA, et al. Viscoelastic property mapping with contact resonance force microscopy. Langmuir 2011;27:13983–7. http://dx.doi.org/10.1021/la203434w.
[35] Gannepalli A, Yablon DG, Tsou AH, Proksch R. Mapping nanoscale elasticity and dissipation using dual frequency contact resonance afm. Nanotechnology 2011;22:355705. http://dx.doi.org/10.1088/0957-4484/22/35/355705.
[36] Haba D, Kaufmann J, Brunner AJ, Resch K, Teichert C. Observation of elastic modulus inhomogeneities in thermosetting epoxies using afm - discerning facts and artifacts. Polymer 2014;55:4032–40. http://dx.doi.org/10.1016/j.polymer.2014.06.030.
[37] Morelle XP, Lani F, Melchior MA, André S, Bailly C, Pardoen T. The elasto-plasticity and fracture behaviour of the rtm6 structural epoxy and impact on the response of woven composites. In: ECCM15-15th European conference on composite materials, Venice (Italy); June 24-28, 2012.
[38] Skordos AA, Partridge IK. Cure kinetics modeling of epoxy resins using a non-parametric numerical procedure. Polym Eng Sci 2001;41:793–805. http://dx.doi.org/10.1002/pen.10777.
[39] Bollinne C, Cuenot S, Nysten B, Jonas AM. Spinodal-like dewetting of thermodynamically-stable thin polymer films. Eur Phys J 2003;E 12:389–96. http://dx.doi.org/10.1140/epje/e2004-00007-6.
[40] Palasantzas G. Roughness spectrum and surface width of self-affine fractal surfaces via the k-correlation model. Phys Rev B 1993;48. http://dx.doi.org/10.1103/PhysRevB.48.14472. 14472–14472.
[41] Tranchida D, Piccarolo S, Soliman M. Nanoscale mechanical characterization of polymers by afm nanoindentations: critical approach to the elastic characterization. Macromolecules 2006;39:4547–56. http://dx.doi.org/10.1021/ma052727j.
[42] Karkanas PI, Partridge IK. Cure modeling and monitoring of epoxy/amine resin systems. i. Cure kinetics modeling. J Appl Polym Sci 2000;77:1419–31. http://dx.doi.org/10.1002/1097-4628(20000815)77.7<1419::AID-APP3>3.0.CO;2-N.
[43] Tranchida D, Kiflie Z, Piccarolo S. Atomic force microscope nanoindentations to reliably measure the Young's modulus of soft matter. In: Méndez-Vilas A, Díaz J, editors. Modern research and educational topics in microscopy. Formatex; 2007.
[44] Brauner C, Block TB, Purol H, Herrmann AS. Microlevel manufacturing process simulation of carbon fiber/epoxy composites to analyze the effect of chemical and thermal induced residual stresses. J Compos Mater 2012;46:2123–43. http://dx.doi.org/10.1177/0021998311430157.
[45] Hexcel. Rtm data sheets [Online; accessed 22.04.15]. 2015., http://www.hexcel.com/Resources/rtm-data-sheets.